# VERTICAL EVACUATION BUILDINGS: SEQUENTIAL EARTHQUAKE AND TSUNAMI ASSESSMENT

C. Cortez[(1)], R. Jünemann[(2), (3)], J. León [(3), (4)]

[(1)] *MsC student, Department of Structural and Geotechnical Engineering, Pontificia Universidad Católica de Chile, cecortez@uc.cl*
[(2)] *Assistant Professor, Department of Structural and Geotechnical Engineering, Pontificia Universidad Católica de Chile, rjunemann@ing.puc.cl*
[(3)] *Researcher, National Research Center for Natural Disaster Management (CIGIDEN), CONICYT/FONDAP/15110017l*
[(4)] *Assistant Professor, Department of Architecture, Universidad Técnica Federico Santa Maria, jorge.leon@usm.cl*

## *Abstract*

Large earthquakes can generate tsunamis that affect cities located in coastal areas, and the most common strategy to reduce fatalities in these cases is to develop horizontal evacuations to sectors that are high and safe. However, in some cases, due to the topology and topography of the cities, the time needed to reach these safe places is too high. Thus, the vertical evacuation to buildings arises as an alternative, which can reduce significantly the evacuation time. For example, in the case of the city of Viña del Mar, in Chile, recent studies show that in the case of an extreme event, 38% of the population is not able to reach safe areas through horizontal evacuation, therefore, the vertical evacuation is an alternative that should be considered.

Vertical evacuation refuges have been considered and implemented in different countries, mainly in Japan, United States and Indonesia, with different typologies: (1) buildings specially constructed as vertical evacuation refuges (towers, buildings or elevated platforms above the expected level of flooding); (2) previously existing buildings, modified or adapted to improve their use for vertical evacuation; and (3) berms or artificial hills. Although there are current regulations in the world that allow the design of vertical evacuation shelters, research on the expected performance of these types of structures under multi-hazard scenarios is scarce. Few studies are available regarding the expected performance of buildings under the sequential seismic-tsunami actions, and even fewer studies consider the scenario in which the building is simultaneously used as a vertical refuge, concentrating large amounts of mass in some area of the building, in case of a strong aftershock.

Thus, the objective of this research is to analyze an existing building in Chile that can serve as a refuge for vertical evacuation. An evaluation of the performance of the structure is carried out by means of a non-linear model that incorporates the reduction of the capacity of the building through a plastic-hinge model based on the smooth histerical model (SHM) considering the sequential earthquake-tsunami action and considering simultaneously that the building is used as a refuge. Results of this research support the vertical evacuation as an alternative to mitigate the effects of a tsunami in Chilean coastal cities.

*Keywords: reinforced concrete wall buildings; vertical evacuation; earthquake and tsunami in sequence; non-linear models; smooth histerical model.*

## 1. Introduction

Large earthquakes can generate tsunamis that affect cities located in coastal areas in different parts of the world. Recent events such as the Great Earthquake in East Japan in 2011 (GEJE) or the Maule earthquake in Chile in 2010 have caused a large number of fatalities and significant damage to the coastal infrastructure [1],[2],[3]. To reduce fatalities caused by the tsunami action in coastal cities, the most common strategy is the horizontal evacuation to elevated areas of the city. However, sometimes the topography and configuration of the city is complex and the time it takes to a person to reach the safe area may not be enough to safe his life. Thus, one mitigation alternative is the vertical evacuation to buildings, which can reduce evacuation time considerably [4]. A vertical evacuation refuge or shelter is defined as a building or mound of earth capable of resisting the effects of a tsunami and capable of safely sheltering people during the emergency. Different types of vertical evacuation shelters have been implemented in countries such as Japan and the United States: (1) buildings specially constructed as vertical evacuation shelters, such as towers, buildings or elevated platforms above the expected level of flooding; (2) existing buildings, modified or adapted to improve their use for vertical evacuation; and (3) artificial hills or hills [5].

Chile is one of the countries frequently affected by major seismic events [6]. León et al. [4] have studied the possible effects of earthquake and tsunami scenarios in coastal cities in Chile, finding that there are 9 vulnerable cities with more than 10% of their population exposed to tsunami hazard, within which is the city of Viña del Mar (10.5%). The great Valparaiso earthquake in 1730, with an estimated magnitude between Mw 9.1 and 9.3 [6] represents an extreme scenario in the area, which destroyed more than 1000 kms of the Chilean coast, from Copiapó to Concepción, and produced a tsunami that hit the coast of Japan. León et al. [4] developed a model of horizontal pedestrian evacuation in Viña del Mar for a tsunami similar to that of 1730. Results of this study showed that approximately 38% of the affected population was not able to arrive to tsunami safe zones trhough horizontal evacuation and that the closest meeting points (PE) can be as far as 30 minutes away (Fig. 1). For this reason, the vertical evacuation alternative arises as a necessary evaluation measure for the case of Viña del Mar.

However, research on the performance of such structures under multiple hazard scenarios is scarce. Regarding seismic behavior, performance evaluation of structures through numerical analysis is well established, typicaly trhough nonlinear time history analysis (DY). Regarding the performance under tsunami actions it is still an area under study, and some of the approaches used for tsunami loads are: nonlinear time history (TDY); variable depth tsunami nonlinear pushover approach (VDPO); and constant depth tsunami nonlinear pushover approach (CDPO). TDY uses the inundation depth ($h(t)$) and the flow velocity ($v(t)$) to calculate the corresponding lateral force at each instant of time ($F_T(t)$). Then, the tsunami force is applied to the structure as a distributed load in the inundation depth. CDPO considers a constant inundation depth ($h$) and the flow velocity ($v$) is increased. The VDPO instead increases the inundation depth linearly to an objective value $h_{max}$ and varies the flow velocity $v$ to maintain a constant Froude number $F_R$ [3],[7].

Within the multi-hazard scenarios, there are even fewer studies that evaluate the performance of buildings under the sequential actions of earthquake and tsunami. Park et al. [8] developed fragility curves for a two-story wooden building subjected to earthquake and tsunami in sequence. The wooden building was modeled as a single degree of freedom (SDoF) system, with capacity and stiffness degradation characterized by the CUREE hysterical response model. They performed nonlinear time history analyses for 44 seismic records and subsequently verified the structural collapse using a tsunami CDPO. This tsunami load was determined according to the FEMA P-646 guidelines [5]. Latcharote and Kai [9] modeled a seven-story reinforced concrete (RC) wall-frame building under a nonlinear time history analysis of earthquake and subsequently CDPO tsunami. Both Park et al. [8] and Latcharote and Kai [9] concluded that the depth of the tsunami flow required to collapse the evaluated structures decreases as the intensity of the earthquake movement of the previous earthquake increases. Additionally, Tagle et al. [10] evaluated the behavior of an 18 story RC wall building by means of nonlinear finite element simulations considering a double pushover analysis. The earthquake pushover is applied until a specific damage state is reached, ant then the tsunami pushover is applied through the VDPO approach. Results showed that the capacity of the building to the tsunami action is not singnificanlty influenced by the previous earthquake damage unless the previous earthquake damage is severe. Rossetto et al. [3] considered a 10-story reinforced concrete building designed as a vertical evacuation structure under a non-linear time history analysis of earthquake and tsunami in sequence. Although this study is the first to present a completely dynamic approach (DY-TDY), it does not consider the scenario in which the building is used simultaneously as a vertical evacuation shelter, i.e., concentrating a large mass in some area of the building.

The objective of this research is to study the behavior of a vertical evacuation building subjected to earthquake and tsunami loading in sequence. This study will evaluate not only the influence of previous earthquake damage in the tsunami capacity of the building, but also the effect of a concentrated mass of people inside the building, when used as vertical evacuation shelter. To reach this objective, a conventional 5-story RC frame building is considered as a case-study building, which is supposed to be located at a critical point in the city of Viña del Mar in Chile. The building is modeled with a non-linear model that incorporates the reduction of the capacity of the building through a plastic-hinge model based on the smooth histerical model (SHM) and a complete dynamic analysis for both earthquake (DY) and tsunami (TDY) is considered. The building is first subjected to two seismic records from the 2010 Maule earthquake that generated different levels of damage to the structure. Then, starting from the damaged condition of the previous earthquake, the tsunami loading is applied which represents the tsunami scenario of the Valparaíso event in 1730. Finally, the condition in which the building is used as a vertical evacuation building is evaluated, that is, with a concentrated mass of people in some area of the building while being subjected to the action of a tsunami and an aftershock of the main earthquake. Finally, the results are analyzed and the feasibility of using buildings currently constructed under Chilean seismic regulations as vertical evacuation shelters is discussed.

## 2. Case-study building

The case study building is a 5-story RC moment-resisting frame building which corresponds to a typical building prototype that has been previously studied [11] and designed considering the Chilean seismic design code Nch433 [12] The building has plan dimensions of $B_{xb}=16\ m$ and $B_{yb}=8\ m$ in each principal direction and a height of $H=17.5\ m$. The building is symmetric and composed by 3 moment resisting frames in the X direction and 2 in the Y direction. A 2D model of a resisting frame in the weakest direction (Y-Z) is considered in this study, which is shown in Fig. 1b. The 8 m beams were designed according to ACI-318 [13] with a dead load of $w_D=150\ kgf/m^2$ and a live load of $w_L=300\ kgf/m^2$ at each story. In the case when the building is considered being used as vertical evacuation shelter, the live load is incremented in $w'_L=500\ [kgf/m^2]$ in the story were the accumulation of people is assumed, which corresponds to the live load of stairs and evacuation routes provided by Chilean provisions Nch1537 [14]. The seismic weight is considered as $P=D+0.25L$ for the primary earthquake, and $P'=D+0.25L+L'$ for the vertical evacuation case.

The materials considered are concrete G25 ($f_c'=25\ MPa$) and reinforcing steel A630-420H ($f_y=420\ MPa$). The building columns have cross section of 70x70 cm, 12 reinforcement bars diameter 25 mm and stirrups diameter 12 mm spaced 12 cm. The beams have cross section of 60x65 cm, with 5 upper reinforcement bars diameter 22 mm and 5 lower reinforcement bars diameter 25 mm. The fundamental period of the complete structure is 0.67 [s] according to Edwards [11], while the fundamental period of the resisting plane considered in this study is 0.76 [s].

For the purpose of this article, the building is assumed to be located at coordinates -33.018970, -71.561625, which correspond to the critical yelow point in Fig. 1a. This location is selected because it corresponds to one of the most critical areas in Viña del Mar that would allow the evacuation of people that won't be able to reach the horizontal evacuation safety points.



 

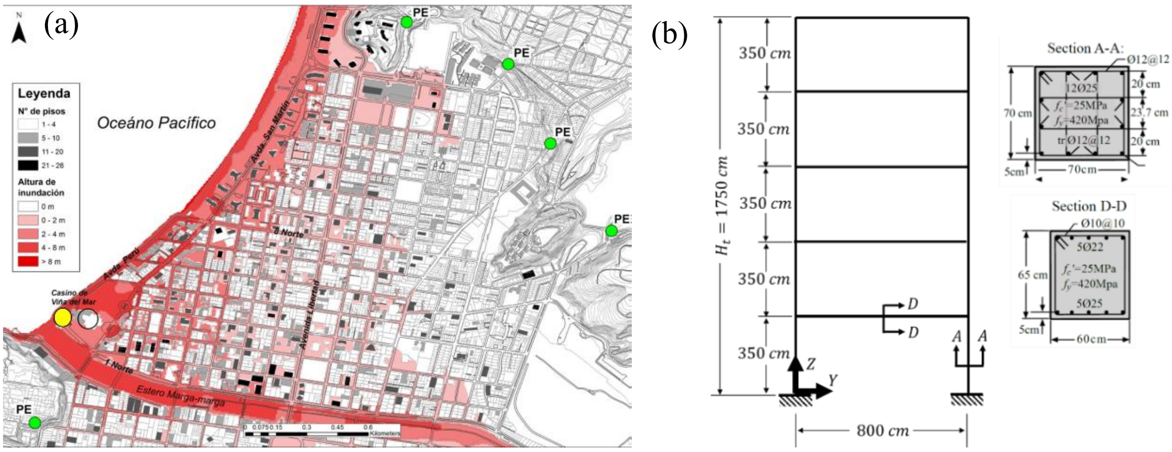


Fig. 1 – (a) Viña del Mar inundation map (modified from León et al. [4]); (b) moment resisting frame of the case-study building considered (modified from Edwards [11]).

## 3. Nonlinear building model

Several studies have implemented the degradation of strength and stiffness in the cyclic behavior of materials [15]. These can be classified into two major groups: polygonal hysteretic model (PHM), and smooth hysteretical model (SHM). On the one hand, the PHM model is based on linear behavior by parts, such as Clough's model [16], Takeda's model [17], and the Park's threeparameters model [18]. On the other hand, the SHM model refers to models with continuous changes in stiffness due to deterioration, such as Bouc-Wen model [19], [20] and Ozdemir's model [21]. Sivaselvan [15] generated a hysterical model for deteriorated inelastic structures that allows incorporating the loss of stiffness and resistance in the constitutive moment ($M$) and curvature ($\phi$) of beams and columns. It is based on the original Bouc-Wen model and requires the incorporation of 6 state variables that are modified at each instant of time: (1) the actual moment $M$; (2) the hysteretic energy $H$; (3) the maximum past positive deformation $\phi^{+}_{max}$; (4) the maximum past negative deformation $\phi^{-}_{max}$; (5) the actual yield positive moment $M^{+}_{y}$; and (6) the actual yield negative moment $M^{-}_{y}$ This model stores important information on deterioration of the material and although it was developed for moment-curvature relations ($M$-$\phi$) it can be applied to any force-deformation pair.

The model proposed by Sivselvan [15] is considered in this study, by means of a moment-rotation relation ($M$-$\theta$) because is a plastic-hinge model. The plastic hinges are modeled within a state space; thus it is necesary to define its variation in time through Eq. 1-7 [15]:

$$\frac{dM_y^{+/-}}{dt} = M_{yo}^{+/-}\left\{\left[1-\frac{\beta_2}{1-\beta_2}\frac{H}{H_{ult}}\right]\cdot\left[-\frac{1}{\beta_1\left(\phi_u^{+/-}\right)^{\frac{1}{\beta_1}}}\left(\phi_{max}^{+/-}\right)^{\frac{1-\beta_1}{\beta_1}}\right]\dot{\phi}_{max}^{+/-}+\left(1-\left(\frac{\phi_{max}^{+/-}}{\phi_u^{+/-}}\right)^{\frac{1}{\beta_1}}\right)\left[1-\frac{\dot{\beta}_2}{(1-\beta_2)H_{ult}}\dot{H}\right]\right\} \tag{1}$$

$$\dot{H} = M\left(\dot{\phi}-\frac{\dot{M}}{R_k K_o}\right) = M\dot{\phi}\left[1-\frac{K_{postyield}+R_k K_{hysteretic}}{R_k K_o}\right] \tag{2}$$

$$\dot{\phi}^{+}_{max} = \dot{\phi}U(\phi-\phi^{+}_{max})U(\dot{\phi}) \tag{3}$$

$$\dot{\phi}^{-}_{max} = \dot{\phi}U(\phi^{-}_{max}-\phi)\left(1-U(\dot{\phi})\right) \tag{4}$$

$$K_{postyield} = a\cdot K_o \tag{5}$$

$$K_{hysteretic} = (R_k-a)K_o\left\{1-\left|\frac{M^*}{M^*_y}\right|^N\left[\frac{1}{2}sgn(M\phi)+\frac{1}{2}\right]\right\} \tag{6}$$



 

$$R_k = \frac{M + \alpha M_y}{(K_o \phi + \alpha M_y)} K_o \tag{7}$$

Where $a$ is the ratio of postyielding to initial stiffness ratio, $\alpha$ is a stiffness degradation parameter, $N$ is power controlling smoothness of the transition from elastic to inelastic range, $\beta_1$ is a degradation parameter based on ductility, and $\beta_2$ is a degradation parameter based on energy. For the case of this study, the following parameters were considered [15]: $a=0.002$; $N=4$; $\alpha=100$; $\beta_1=\beta_2=0.2$.

Based on the moment-curvature relations for beams and columns, the yield moment $M_y$, yield curvature $\phi_y$ and ultimate curvature $\phi_u$ were obtained. There are several studies to obtain the yield rotation $\theta_y$ and ultimate rotation $\theta_u$ from the section curvature. According to Park and Paulay [21], the element rotation is $\theta_A^B = \int_A^B \phi \, dx$ thus the yield rotation is $\theta_y = \phi_y \cdot \frac{L}{2}$ and the ultimate rotation is $\theta_u = \theta_y + (\phi_u - \phi_y) \cdot L_p$, where $L$ is the length of a cantilever element and $L_p$ is the plastic hinge length wich is estimated as half the section height. According to Panagiotkos and Fardis [22], the flexural component of the deformation can be calculated as $\theta_{y,f} = \phi_y \cdot \frac{L_s}{3}$ where $L_s$ is the inflexion length. Additioally, Haselton and Deirlein [23] developed 255 tests in RC columns and found that the total yield deformation is approximately twice the flexural deformation i.e. $\theta_y = 2\theta_{y,f}$, Finally, Fardis et al. [24] observed through 900 tests in rectangular sections that the average plastic deformation for beams was $\theta_{cap} = 0.07\ [rad]$ and $\theta_{cap} = 0.05\ [rad]$ for columns.

Therefore, yield flexural rotation was determined based on Panagiotkos and Fardis [22], considering a length of half the span $L_s = L/2$, and the total yield deformation twice the flexural deformation according Haselton and Deirlein [23]. The ultimate deformation based on the empirical results of Fardis et al. [24] were calculated using $\theta_u = \theta_y + \theta_{cap}$ . The values used are show in Table 1, and Fig. 2 shows the behavior of the plastic hinges for beams and columns subjected to a cyclic displacement of increasing magnitude.

Table 1. Moment-rotation parameters of beams and column

| Element | $M_y\ [tonf\ cm]$ | $\phi_y\ [rad/cm]$ | $L\ [cm]$ | $L_s\ [cm]$ | $\theta_y\ [rad]$ | $\theta_u\ [rad]$ |
|---|---|---|---|---|---|---|
| Beams | 5386 | $4.5 \cdot 10^{-5}$ | 800 | 400 | 0.01 | 0.072 |
| Columns | 5811 | $4.4 \cdot 10^{-5}$ | 350 | 175 | 0.005 | 0.055 |

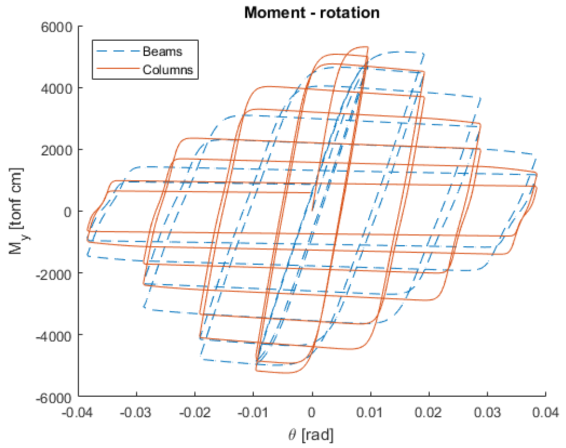


Fig. 2 – Moment-rotation relation for beams and columns in the nonlinear model


 

The numerical model of the structure was implemented in Matlab [25] considering plastic hinges in the extreme of the beams of the first three stories, and in the columns of the first and second stories (Fig. 4), considering the previously described moment-rotation relation (Fig. 2). The rest of the elements in the models were modeled with linear-elastic behavior due to the high computational cost of including plastic hinghes in all elements. Frame type elements were used for beams and columns with the material properties indicated in section 2. Rayleigh damping (mass and proportional stiffness $\boldsymbol{C}=\alpha \boldsymbol{M}+\beta \boldsymbol{K}$) was used where the coefficients $\alpha$ and $\beta$ as those that produce a 3% damping in 1.5 and 0.25 times the fundamental period.

## 4. Earthquake and tsunami loads in sequence

The analysis of the behavior of the structure under earthquake and tsunami loadings is divided into three part: (1) seismic load, the structure is subjected to two seismic records that produce different damage levels; (2) tsunami load, the structure starts from a damaged condition (1) and then is subjected to the tsunami forces; and (3) tsunami and aftershock: the structure damaged by an initial seismic record is used as the initial condition and the structure is subjected to the joint tsunami action and aftershock with a concentrated mass of people inside the building. Additionally, an elastic model is generated for each loading case for reference purposes.

### 4.1 Sesimic load

The seismic records considered in this study correspond to the 2010 earthquake event. Two stations located in the city of Viña del Mar were selected: Viña Centro (VC) and Viña El Salto (VS). Both with a very similar maximum ground acceleration PGA, the first with PGA=0.33 g, while the second with PGA=0.35 g. Although the elastic model has a fundamental period of $T = 0.76\ s$, the generated nonlinear models have a longer fundamental period $T \approx 1.3 - 1.4\ s$. Fig. 3a shows the ground acceleration in time for both seismic rectods, while Fig. 3b shows the spectral acceleration and the periods of interest.

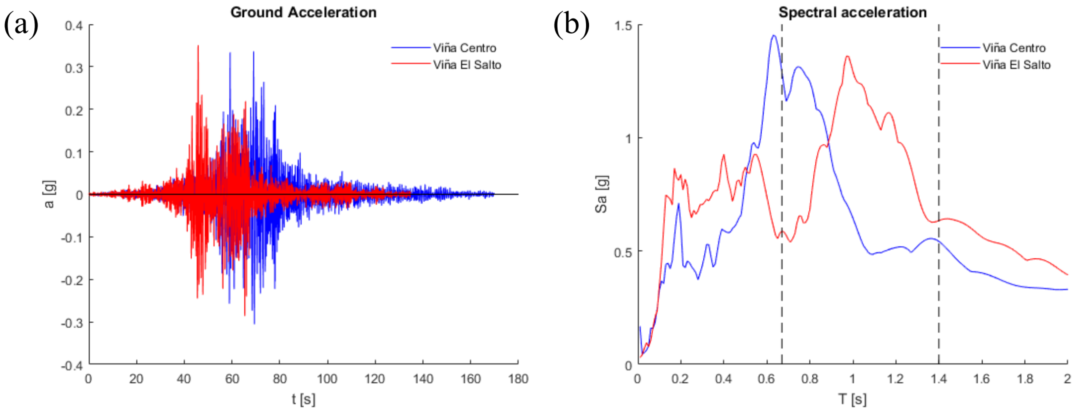


Fig. 3 – Ground motions: a) soil acceleration; and b) pseudo-acceleration response spectra.

### 4.2 Tsunami load

To calculate the lateral tsunami force proposed by Foster et al. [7] to estimate forces in rectangular bodies partially immersed in quasi-static flows, it is required to know the inundation depth *h(t)*, and flow speed *v(t)*, at each time instant. These parameters were obtained from a simulation of the 1730 Valparaiso tsunami carried out by Carvajal et al. [6] at the location of the building indicated in section

The tsunami force $F_T(t)$ per unit of width $b$ at each time instant is calculated using Eq. 8 proposed by Foster et al. [7] according to Qi et al. [26]

$$\frac{F_T(t)}{b} = sgn\big(v(t)\big)\begin{cases} 0.5\, C_D\, \rho\, v^2 h\,, & F_r < F_{rc} \\ \lambda\, \rho\, g^{1/3}\, u^{4/3} h^{4/3}, & F_r \geq F_{rc} \end{cases} \quad (8)$$



 

Where $C_D$ is the drag coefficient, $\rho$ is the water density ($1.2\ ton/m^3$), $sgn(v)$ is the sign function of the flow speed, $g$ is the acceleration of gravity, $\lambda$ is the 'choking ratio', $F_r = v/\sqrt{gh}$ is the Froude number of the flow and $F_{rc}$ is the Froude number threshold, which denotes subcritical ($F_r < F_{rc}$) and choked ($F_r \geq F_{rc}$) conditions for the steady-state flow. There are equations to define $F_{rc}, C_D, \lambda$ based on the 'blocking ratio' $b/w$, parameter that represents the urban density of the building. In the study by Qi et al. [26], $b$ corresponds to the building width, while $w$ corresponds to the channel width. Rosseto et al. [3] and Petrone et al. [27] used a 'blocking ratio' $b/w = 0.6$ with the corresponding parameters $C_D = 4.7$, $\lambda = 2.0$, $F_{rc} = 0.32$, which are also used in this study. Fig. 4a-d show the data for the tsunami simulation and Fig. 4e shows the tsunami force obtained from these parameters, where $p_D(t) = \frac{2F_T(t)}{h(t)}$ is the base of the triangular pressure distribution.

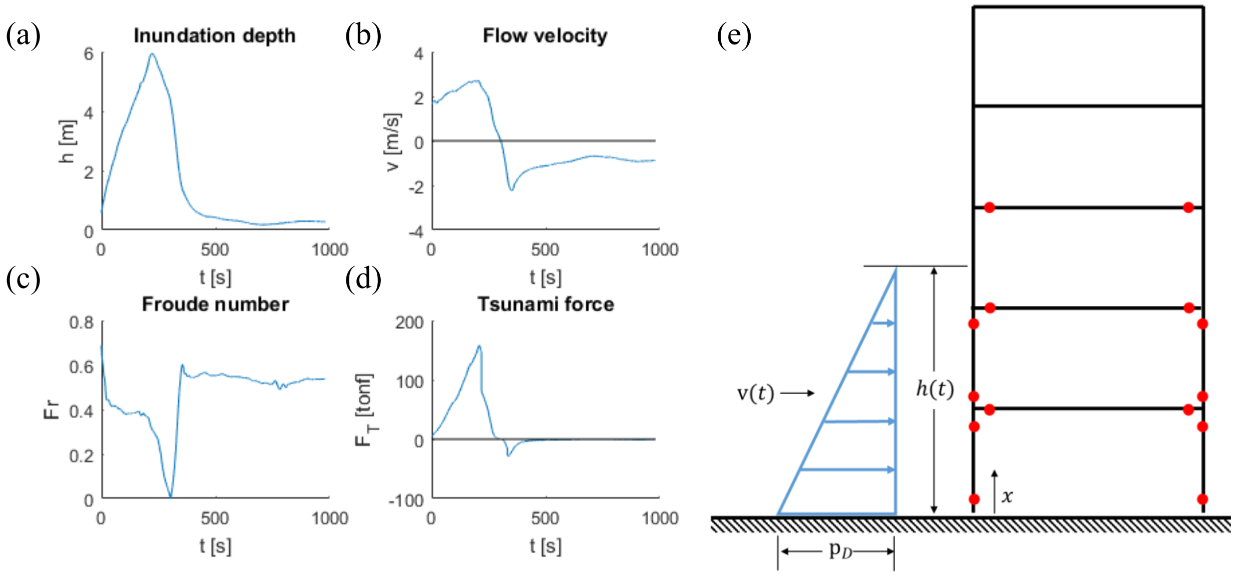


Fig. 4 – Tsunami simulation: a) inundation depth; b) flow velocity; c) Froude number; d) tsunami force; and e) tsunami force application to the building.

To implement the tsunami load in the building model, it is required to calculate the nodal forces $F_e$ generated by the distributed tsunami force in Fig. 4e. For each column subjected to the tsunami action, the distributed load $q(x,t)$ is calculated at each time instant and then the nodal forces $F_e$ are calculated from the interpolation functions Eq. 9-14:

$$N_1 = 1 - \frac{3x^2}{L^2} + \frac{2x^3}{L^3} \tag{9}$$

$$N_2 = x - 2\frac{x^2}{L} + \frac{x^3}{L} \tag{10}$$

$$N_3 = \frac{3x^2}{L^2} - \frac{2x^3}{L^3} \tag{11}$$

$$N_4 = -\frac{x^2}{L} + \frac{x^3}{L^2} \tag{12}$$

$$N_e = [N_1\ N_2\ N_3\ N_4] \tag{13}$$

$$F_e = -\int_0^L N_e(x)^T q_e(x,t)dx \tag{14}$$

4.3 Tsunami and aftershock

In the case when the building is used as a vertical evacuation shelter, the structure was subjected to the action of the tsunami and aftershock simultaneously. To do this, the same seismic records of Viña Centro and Viña El Salto were used, but half of their magnitude, simulating aftershocks of the main event. However, both tsunami and aftershock loads have a different time discretization and total duration. The tsunami load has a duration of 16 minutes and is discretized every 0.15 seconds, while the earthquake has an approximate duration of 2 minutes discretized in 0.005 seconds for VS and 0.01 for VC. For this reason, it was necessary to interpolate the tsunami record and define an earthquake start time. It can be depicted from Fig. 4 that the highest tsunami force occurs between 100 and 300 seconds, so for the purpose of this study it was supposed that the aftershock starts after the first 100 seconds of the tsunami. Regarding the location of the refugees, as the depth of flooding shown in Fig. 4 does not exceed 6 $m$, the refugees are supposed to be concentrated on the third, fourth or fifth storey, since this way people is above the flooding depth.

## 5. Results

This section shows the comparison of some engineering demand parameters (EDP) like the maximum story displacement and the maximum interstory drift when the structure is subjected to the loads presented in section 4. Results also include the moment-rotation relations of the most critical plastic hinges. Additionally, the structure reduction capacity is cuantified by means of the state variable related to the actual yield moment $M_y$ at the end of the analysis, in order to calculate the residual capacity of the plastic hinge as the ratio between the initial yield moment and the actual yield moment $R = \frac{M_{yf}}{M_{yo}}$.

5.1 Seismic load

Results in this section compare the response of the elastic structure (E), and inelastic structure (IB) subjected to the Viña Centro (VC) and Viña el Salto (VS) records. It is evident form Fig. 5 that the elastic structure has a larger response for the VS record (E-VS), while the inelastic model has a larger response for the VC record (IB-VC). This occurs because the pseudo-acceleration response spectra (Fig. 3b) for the elastic case ($T = 0.76\ [s]$) is larger for VS than for VC, while for the inelastic case ($T \approx 1.3\ [s]$) the opposite occurs, i.e., the response is much larger for VC than for VS. It is also possible to observe that for the elastic models the maximum interstory drift occurs at the second story. In the case of inelastic models, the maximum drift for IB-VS occurs at the first story, while for IB-VS the maximum drift occurs at the second story, as was the case of the elastic models.

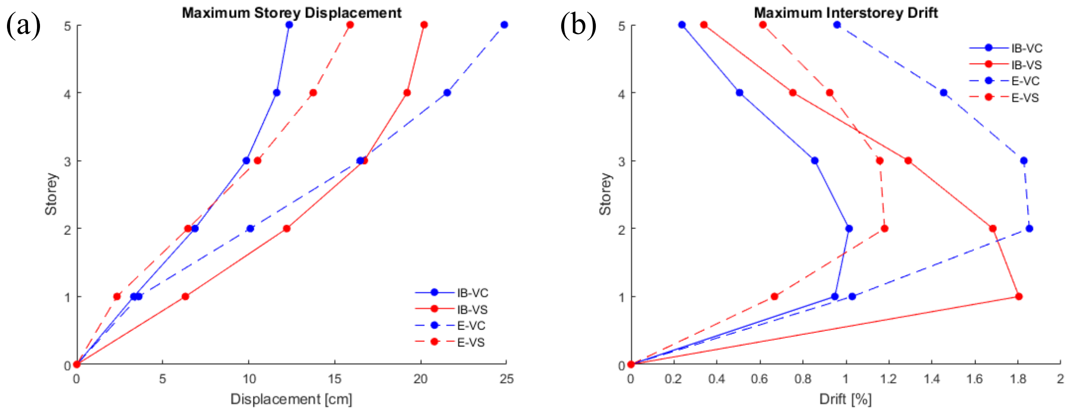


Fig. 5 – Response of the structure for seismic load: a) maximum story displacement; and b) maximum interstory drift.

Fig. 6a-d shows the moment-rotation response history of the plastic hinges at the first story. It is posible to note that in the IB-VC case the structure remains within the elastic range, while in the IB-VS case inelastic excursions occur, particularly in the lower plastic hinge of the first-story columns, which causes structural damage. This plastic-hinge has a residual capacity $R = 82.3$ %, while for the IB-VC case the residual capacity is $R = 98.6$ %.

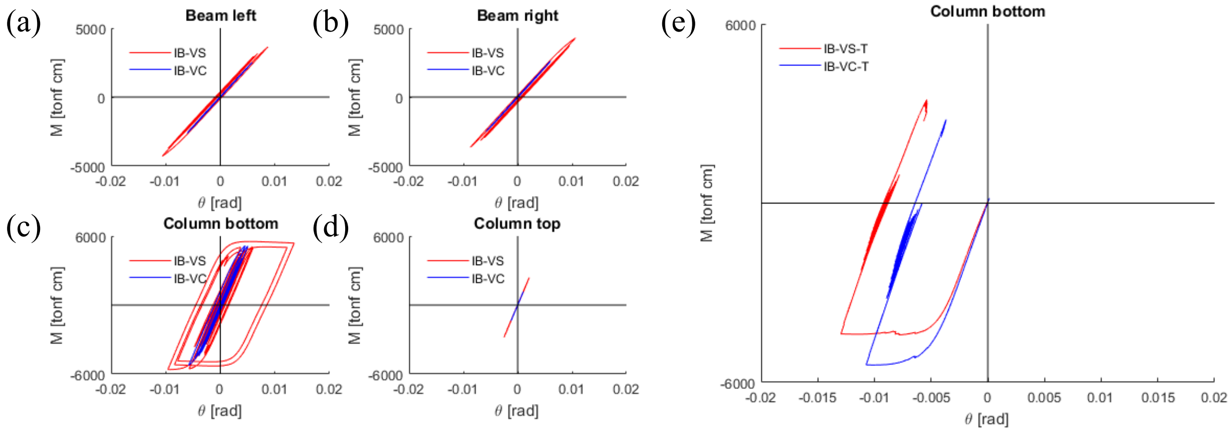


Fig 6. Response of the first story plastic hinges. For seismic load: (a) left side beam; (b) right side beam; (c) column bottom; (d) column top. For tsunami load (e) column bottom.

5.2 Tsunami load

Four cases are presented in this section: the elastic structure subjected to the tsunami action (E-T); the inelastic structure subjected to the tsunami action (IB-T); and the inelastic structure subjected to the tsunami action but with previous earthquake damage due the Viña Centro record (IB-VC-T), and due to Viña El Salto record (IB-VS-T). Fig. 7 shows that the structure has a significantly lower response in the elastic case (E-T) than the three inelastic cases, even when no previous earthquake is considered (IB-T). This occurs because the elastaic model does not consider the damage concentration at the first story columns due to the tsunami distributed load. Results show that the case IB-VC-T has a very similar response than the case without previous earthquake (IB-T), while the case IB-VS-T has a roof displacement 17% larger than the IB-VC-T case, and a maximum interstory drift also 17% larger. The behavior of the plastic hinge at the bottom of the first story column is shown in Fig. 6e, where the IB-VS-T case shows a yield moment lower than the IB-VC-T case due to the previous earthquake damage. The residual capacity for the IB-VS-T case is $R = 75$ %, while for the IB-VC-T case is $R = 93$ %.

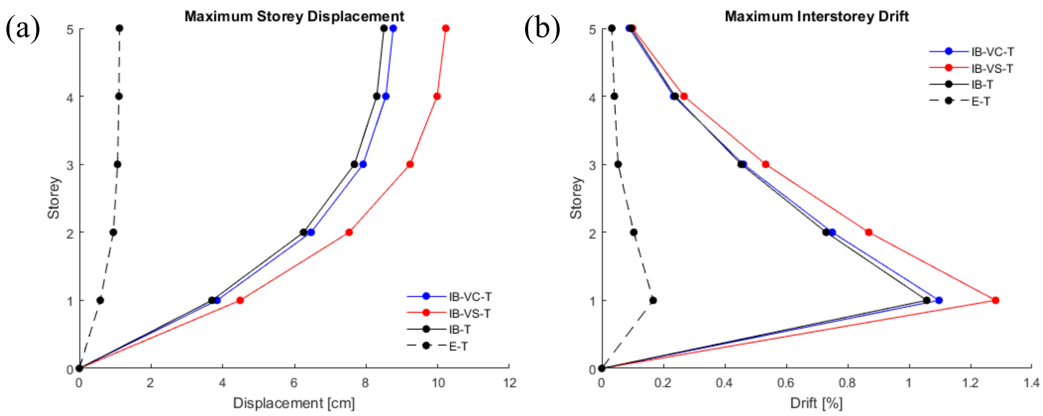


Fig. 7 – Response of the structure for tsunami load: a) maximum story displacement; and b) maximum interstory drift

5.3 Tsunami and aftershock

This section considers the situation when the building is used as vertical evacuation shelter and is subjected to the simultaneous action of the tsunami and the aftershock. Different cases are considered in this section regarding the location of the refugees inside the building, which is represented as a concentrated mass in a story: third, fourth or fifth story. Considering both seismic events, a total of six different cases are evaluated, which are shown in Table 2. The table also shows the residual capacity of the critical plastic hinge, which corresponds to the one located at the bottom of the first story column. Results show that the three VS cases produce significantly larger damage that the VC cases, while the cases were the concentrated mass is located do not produce significant differences. Fig. 8 shows that the maximum interstory drift occurs at the first story, and that for all the cases with VS record the response is much larger than for the VC case.

Table 2. Cases for tsunami and aftershock.

| Case | Location of the concentrated mass | Seismic Event | Residual Capacity [%] |
|---|---|---|---|
| **VE3-VS** | Third story | Viña el Salto | 70.8 |
| **VE4-VS** | Fourth story | Viña el Salto | 71.0 |
| **VE5-VS** | Fifth story | Viña el Salto | 71.1 |
| **VE3-VC** | Third story | Viña Centro | 91.8 |
| **VE4-VC** | Fourth story | Viña Centro | 91.8 |
| **VE5-VC** | Fifth story | Viña Centro | 91.7 |

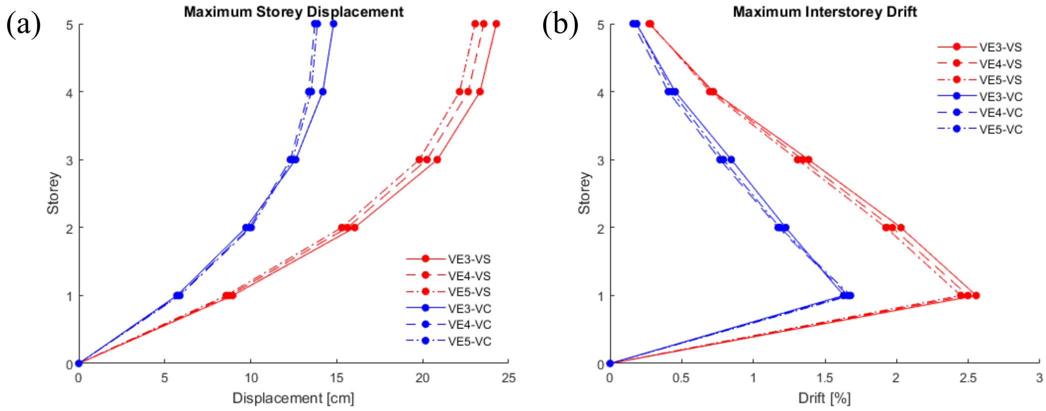


Fig. 8 – Response of the structure for the case of tsunami and aftershock: a) maximum story displacement; and b) maximum interstory drift

## 5. Concluding remarks

This research studies the behavior of a RC building used as vertical evacuation shelter and subjected to multi-hazard earthquake and tsunami in sequence. The case-study building considered is a 5 story RC frame building located at a critical point in Viña del Mar, Chile. The building was modeled considering a smooth histerical model (SHM) for the plastic hinges in beams and columns, and complete nonlinear dyamic analysis for both earthquake (DY) and tsunami (TDY).

Results show that the when the previous earthquake damage is low, the residual capacity of the critical element is approximately 92%, while it reduces to approximately 70% in the case when the previous earthquake damage is higher. Additionally, results show that the location of the refugees inside the building does not have a significant effect in the structural response.

Results also show that using elastic building models to represent the behavior of the structure for tsunami actions significantly underestimates the structural response because it neglects the damage concentration at the first story columns due to the tsunami distributed load. For the tsunami loads, the inelastic excursions of the first story columns are significant, which traduces in differences of an order of magnitude between the response obtained with elastic versus inelastic models.

Regarding the case-study building considered, it can be concluded that RC buildings designed considering the Chilean seismic design provisions present an adequate performance under the simultaneous effect of tsunami and earthquake when used as vertical evacuation shelters, with a residual capacity larger than 70%.

Finally, it is concluded that this type of building presents an alternative for vertical evacuation strategies. More research needs to be done regarding the behavior of reinforced concrete buildings subjected to the earthquake and tsunami actions, including other effects that were not discussed in this study, such as soil-structure interaction, the impact of debris and the buoyancy forces, among others.

## 6. Acknowledgements

This research has been funded by the National Science and Technology Council of Chile, CONICYT, under grant Fondecyt 11170514 and the Research Center for Integrated Disaster Risk Management (CIGIDEN), CONICYT/FONDAP/15110017. The authors gratefully acknowledge the support provided by Alejandra Gubler from CIGIDEN and Professor José Luis Almazán from PUC.

## 7. References

[1] Fraser, S., Raby, A., Pomonis, A., Goda, K., Chian, S. C., Macabuag, J., … Sammonds, P. (2013). Tsunami damage to coastal defences and buildings in the March 11th 2011 Mw9.0 Great East Japan earthquake and tsunami. *Bulletin of Earthquake Engineering*, *11*(1), 205–239. https://doi.org/10.1007/s10518-012-9348-9

[2] Macabuag, J., Raby, A., Pomonis, A., Nistor, I., Wilkinson, S., & Rossetto, T. (2018). Tsunami design procedures for engineered buildings: A critical review. *Proceedings of the Institution of Civil Engineers: Civil Engineering*, *171*(4), 166–178. https://doi.org/10.1680/jcien.17.00043

[3] Rossetto, T., De la Barra, C., Petrone, C., De la Llera, J. C., Vásquez, J., & Baiguera, M. (2019). Comparative assessment of nonlinear static and dynamic methods for analysing building response under sequential earthquake and tsunami. *Earthquake Engineering and Structural Dynamics*, *48*(8), 867–887. https://doi.org/10.1002/eqe.3167

[4] León, J., Zamora, N., Castro, S., Jünemann, R., Gubler, A., & Cienfuegos, R. (2019). *Evacuación vertical como medida de mitigación del riesgo de tsunamis en Chile*.

[5] Federal Emergency Management Agency. (2008). Guidelines for Design of Structures for Vertical Evacuation from Tsunamis.

[6] Carvajal, M., M. Cisternas, and P. A. Catalán (2017), Source of the 1730 Chilean earthquake from historical records: Implications for the future tsunami hazard on the coast of Metropolitan Chile, J. Geophys. Res. Solid Earth, 122, 3648–3660, doi:10.1002/ 2017JB014063.

[7] Foster, A. S. J., Rossetto, T., & Allsop, W. (2017). An experimentally validated approach for evaluating tsunami inundation forces on rectangular buildings. *Coastal Engineering*, *128*, 44–57. https://doi.org/10.1016/j.coastaleng.2017.07.006

[8] Park, S., Van De Lindt, J. W., Cox, D., Gupta, R., & Aguiniga, F. (2012). Successive earthquake-tsunami analysis to develop collapse fragilities. *Journal of Earthquake Engineering*, *16*(6), 851–863. https://doi.org/10.1080/13632469.2012.685209

[9] Latcharote, P., & Kai, Y. (2014). Nonlinear structural analysis of reinforced concrete buildings suffering damage from earthquake and subsequent tsunami. *NCEE 2014 - 10th U.S. National Conference on Earthquake Engineering: Frontiers of Earthquake Engineering*, (January). https://doi.org/10.4231/D33J39197

[10] Tagle S.J., Jünemann R., Vásquez J.A., de la Llera J.C., Baiguera M. (2020): Performance of a Reinforced Concrete (RC) Wall Building Subjected to Sequential Earthquake and Tsunami Loading. *Engineering Structures*, Under review.



 

[11] Edwards, J. J. (2019). Optimization of a self-centering frictional damper (SCFD) and its application to non-linear structures. *Master of Science thesis*, Pontificia Universidad Católica de Chile.

[12] NCh433. (1996). Earthquake Resistant Design of Buildings (in Spanish). *Instituto Nacional de Normalización (INN), Santiago, Chile.*

[13] ACI-318. (2014). Building code requirements for structural concrete and commentary (318-14). *American Concrete Institute (ACI), Detroit, Michigan.*

[14] NCh1537. (2009). Structural design Dead and live loads (in Spanish). *Instituto Nacional de Normalización (INN), Santiago, Chile.*

[15] Sivaselvan, M. V., & Reinhorn, A. M. (2000). Hysteretic models for deteriorating inelastic structures. *Journal of Engineering Mechanics*, *126*(6), 633–640. https://doi.org/10.1061/(ASCE)0733-9399(2000)126:6(633)

[16] Clough, R. W. (1966). Effects of stiffness degradation on earthquake ductility requirement. Rep. No. 6614, struct. and Mat. Res., University of California, Berkeley, Calif.

[17] Takeda, T., Sozen, M. A., and Nielsen, N. N. (1970). Reinforced concrete response to simulated earthquakes. *J. Struct. Div.*, ASCE, 96(12), 2557–2573.

[18] Bouc, R. (1967). Forced vibration of mechanical systems with hysteresis. *Proc., 4th Conf. on Non-linear Oscillations*.

[19] Wen, Y.-K. (1976). Method for random vibration of hysteretic systems. *J. Engrg. Mech. Div.*, ASCE, 102(2), 249–263.

[20] Ozdemir, H. (1976). Nonlinear transient dynamic analysis of yielding structures. PhD dissertation, University of California, Berkeley, Calif.

[21] Park, R., and T. Paulay, T. (1975). Reinforced Concrete Structures. A Wiley-Interscience Publication, pp. 740-757.

[22] Panagiotakos, T. B. and Fardis, M. N. (2001). Deformations of Reinforced Concrete at Yielding and Ultimate. *ACI Structural Journal*, Vol. 98, No. 2, March-April 2001, pp. 135-147.

[23] Haselton, C., & Deierlein, G. (2007). Assesing Seismic Collapse Safety of Modern Reinforced Concrete Moment Frame Buildings. (156).

[24] Fardis, M. N. and Biskinis, D. E. (2003). Deformation Capacity of RC Members, as Controlled by Flexure or Shear, *Otani Symposium*, 2003, pp. 511-530.

[25] The MathWorks, I. (2019). Matlab 2019b. Available for download at: http://www.mathworks.com/ (Accessed on 31 Jan 2019.).

[26] Qi ZX, Eames I, Johnson ER. Force acting on a square cylinder fixed in a freesurface channel flow. J Fluid Mech 2014;756:716–27

[27] Petrone, C., Rossetto, T., & Goda, K. (2017). Fragility assessment of a RC structure under tsunami actions via nonlinear static and dynamic analyses. *Engineering Structures*, *136*, 36–53. https://doi.org/10.1016/j.engstruct.2017.01.013



 